ARL-TR-9898 • MAR 2024

Using Linear Parameter-Varying Models to Represent Nonlinear Flight Dynamics

by Joshua T Bryson and Benjamin C Gruenwald

NOTICES

Disclaimers

ARL-TR-9898 ● MAR 2024

Using Linear Parameter-Varying Models to Represent Nonlinear Flight Dynamics

Joshua T Bryson and Benjamin C Gruenwald
DEVCOM Army Research Laboratory

REPORT DOCUMENTATION PAGE

Form Approved
OMB No. 0704-0188

1. REPORT DATE *(DD-MM-YYYY)*	**2. REPORT TYPE**	**3. DATES COVERED (From - To)**
March 2024	Technical Report	1 Dec 2023–31 Jan 2024

4. TITLE AND SUBTITLE
Using Linear Parameter-Varying Models to Represent Nonlinear Flight Dynamics

5a. CONTRACT NUMBER

5b. GRANT NUMBER

5c. PROGRAM ELEMENT NUMBER

6. AUTHOR(S)
Joshua T Bryson and Benjamin C Gruenwald

5d. PROJECT NUMBER

5e. TASK NUMBER

5f. WORK UNIT NUMBER

7. PERFORMING ORGANIZATION NAME(S) AND ADDRESS(ES)
DEVCOM Army Research Laboratory
ATTN: FCDD-RLA-WD
Aberdeen Proving Ground, MD 21005

8. PERFORMING ORGANIZATION REPORT NUMBER
ARL-TR-9898

9. SPONSORING/MONITORING AGENCY NAME(S) AND ADDRESS(ES)

10. SPONSOR/MONITOR'S ACRONYM(S)

11. SPONSOR/MONITOR'S REPORT NUMBER(S)

12. DISTRIBUTION/AVAILABILITY STATEMENT
DISTRIBUTION STATEMENT A. Approved for public release; distribution is unlimited.

13. SUPPLEMENTARY NOTES
primary author's email: <joshua.t.bryson.civ@army.mil>.
ORCIDs: Joshua T. Bryson, 0000-0002-0753-6823; Benjamin C. Gruenwald, 0000-0003-3968-5070

14. ABSTRACT
This report presents a convenient model formulation for representing vehicle dynamics across a wide flight envelope. This approach has advantages in the design of gain-scheduled controllers. An example nonlinear model is provided and the process for trimming and linearizing the nonlinear model is presented. Several linear models typically used to represent the dynamics of aerospace vehicles are discussed along with a method to identify the dominant modes of motion. The presented model formulation is then validated against the full nonlinear model in simulation for comparison.

15. SUBJECT TERMS projectile flight dynamics, model trimming, model linearization, linear parameter-varying model, longitudinal short-period model, lateral-directional model, Weapons Sciences

16. SECURITY CLASSIFICATION OF:			**17. LIMITATION OF ABSTRACT**	**18. NUMBER OF PAGES**	**19a. NAME OF RESPONSIBLE PERSON**
					Joshua T Bryson
a. REPORT	**b. ABSTRACT**	**c. THIS PAGE**			**19b. TELEPHONE NUMBER (Include area code)**
Unclassified	Unclassified	Unclassified	UU	36	410-306-1939

Standard Form 298 (Rev. 8/98)
Prescribed by ANSI Std. Z39.18

Contents

List of Figures

List of Tables

1. Introduction

The flight dynamics of projectiles are fundamentally nonlinear and coupled in different planes of motion. In addition, the aerodynamics that supply coefficient data specific to the projectile flight body vary across flight condition and can be highly nonlinear with respect to parameters such as Mach number or angle of attack, α. As a result, detailed models that precisely predict projectile flight behavior can become complex. At the same time, many of the well-established control design techniques are developed in a linear space. This requires the linearization of nonlinear flight dynamics, which is only valid in a limited flight regime close to the particular linearization condition. A popular approach to address this challenge is gain scheduling–that is, designing a schedule of control gains tuned for a family of linear models that appropriately span the flight envelope. The result is a flight controller that is still able to leverage the techniques of linear control design by incrementally capturing the nonlinear vehicle dynamics. While some challenging applications may require the use of more complicated nonlinear control strategies, gain scheduling is appropriate often and remains among the predominant flight control methods.[1–4]

Linear parameter-varying (LPV) models are a powerful tool in the design of gain-scheduled autopilots. These models allow the representation of nonlinear vehicle dynamics as a compact family of linear time-invariant (LTI) systems whose coefficients vary with certain parameters (typically flight conditions such as airspeed and altitude). This parameter-dependent representation facilitates the use of robust linear control techniques while still capturing much of the inherent nonlinear behavior of the vehicle dynamics. In the context of gain-scheduled autopilot design, LPV models aid in the synthesis of controllers that change with flight conditions, thereby enhancing the performance and stability of the vehicle across its entire operating envelope.[4] This approach is particularly useful for modern aircraft that operate over a wide range of conditions and require high-performance control systems.

An additional benefit to the LPV model formulation is a convenient, standardized packaging of the linear models along with trimming offset terms that can facilitate sharing of data with collaboration partners. Modern engineering software packages such as MATLAB have built-in LPV data structures that lower the chance of mistakes when sharing data between different groups.

This report is organized as follows:

1. Details of the chosen LPV approach are presented,
2. An example nonlinear vehicle model is summarized,
3. The process for trimming a model is described,
4. The model linearization approach and 6-degree-of-freedom (6DoF) linear models are presented for both the body-frame and stability-frame coordinates,
5. A modal analysis is performed on the linearized system and decoupled dynamics models for the longitudinal and lateral-directional dynamics are described,
6. Finally, simulations of the nonlinear and LPV models are compared for validation.

2. Approach

A model of the 6DoF equations of motion and full nonlinear aerodynamics is developed using Simulink, a desired flight envelope for the projectile is defined, and a grid is created of discrete points of flight conditions across the flight envelope. Then, using MATLAB and Simulink tools, the nonlinear model is trimmed and linearized at each point within the gridded flight envelope. The trimming process solves for the set of control deflections that result in quasi-steady-state flight (i.e., aerodynamic moments are zero) matching the flight conditions for each point. The linearization process then identifies a linear approximation for the dynamic system at each trim point.

The result is a family of linear models incrementally scheduled across the flight envelope that, when combined, describe the behavior of the nonlinear system to a reasonable degree of accuracy. Formally, this is known as an LPV model. An LPV model constructed in this way (i.e., using LTI models) does not capture the transient behaviors between model sample points or flight in non-trim conditions, potentially neglecting important nonlinearities and coupling terms that can affect the system behavior.

In contrast to this linearization approach, the *State Transformation* method[5] has been used to provide an exact transformation between the original nonlinear system and an associated LPV model, avoiding the approximation errors. Due to the inclusion of additional terms and integration of the control input, the resulting LPV model does not depend on the specific operating point and accounts for any offequilibrium conditions. However, this State Transformation approach is more involved and beyond the scope of this work. It is noted here for reference, in case the LTI model approach is insufficient for a future application.

3. Nonlinear Model Description

This section presents the nonlinear equations associated with a generic tail-controlled projectile vehicle. While a more thorough treatment can be found in previous work,[1] we provide a brief overview of the nonlinear equations used to describe the projectile model. To begin, the 6DoF equations of motion are given by

$$\begin{bmatrix} \dot{x} \\ \dot{y} \\ \dot{z} \end{bmatrix} = \begin{bmatrix} \mathrm{c}_\theta \mathrm{c}_\psi & \mathrm{s}_\phi \mathrm{s}_\theta \mathrm{c}_\psi - \mathrm{c}_\phi \mathrm{s}_\psi & \mathrm{c}_\phi \mathrm{s}_\theta \mathrm{c}_\psi + \mathrm{s}_\phi \mathrm{s}_\psi \\ \mathrm{c}_\theta \mathrm{s}_\psi & \mathrm{s}_\phi \mathrm{s}_\theta \mathrm{s}_\psi + \mathrm{c}_\phi \mathrm{c}_\psi & \mathrm{c}_\phi \mathrm{s}_\theta \mathrm{s}_\psi - \mathrm{s}_\phi \mathrm{c}_\psi \\ -\mathrm{s}_\theta & \mathrm{s}_\phi \mathrm{c}_\theta & \mathrm{c}_\phi \mathrm{c}_\theta \end{bmatrix} \begin{bmatrix} u \\ v \\ w \end{bmatrix}, \tag{1}$$

$$\begin{bmatrix} \dot{\phi} \\ \dot{\theta} \\ \dot{\psi} \end{bmatrix} = \begin{bmatrix} 1 & \mathrm{s}_\phi \mathrm{t}_\theta & \mathrm{c}_\phi \mathrm{t}_\theta \\ 0 & \mathrm{c}_\phi & -\mathrm{s}_\phi \\ 0 & \mathrm{s}_\phi/\mathrm{c}_\theta & \mathrm{c}_\phi/\mathrm{c}_\theta \end{bmatrix} \begin{bmatrix} p \\ q \\ r \end{bmatrix}, \tag{2}$$

$$\begin{bmatrix} \dot{u} \\ \dot{v} \\ \dot{w} \end{bmatrix} = \frac{1}{m} \begin{bmatrix} X - mg\mathrm{s}_\theta \\ Y + mg\mathrm{s}_\phi \mathrm{c}_\theta \\ Z + mg\mathrm{c}_\phi \mathrm{c}_\theta \end{bmatrix} - \begin{bmatrix} 0 & -r & q \\ r & 0 & -p \\ -q & p & 0 \end{bmatrix} \begin{bmatrix} u \\ v \\ w \end{bmatrix}, \text{ and} \tag{3}$$

$$\begin{bmatrix} \dot{p} \\ \dot{q} \\ \dot{r} \end{bmatrix} = \vec{I}^{-1} \begin{bmatrix} L \\ M \\ N \end{bmatrix} - \vec{I}^{-1} \begin{bmatrix} 0 & -r & q \\ r & 0 & -p \\ -q & p & 0 \end{bmatrix} \vec{I} \begin{bmatrix} p \\ q \\ r \end{bmatrix}. \tag{4}$$

Using Fig. 1 to illustrate the relation between the body-fixed reference frame and the inertial Earth frame, we note in Eqs. 1–4 that $[x, y, z]^\mathrm{T}$ are the center-of-gravity positions relative to the inertial Earth frame along the x_E, y_E, and z_E axes, respectively; $[\phi, \theta, \psi]^\mathrm{T}$ are the Euler angles for roll, pitch, and yaw describing the angular orientation (or attitude); $[u, v, w]^\mathrm{T}$ are the body-fixed linear (or translational) velocities acting in the x_b, y_b, and z_b directions, respectively; and $[p, q, r]^\mathrm{T}$ are the body-fixed angular (or rotational) velocities acting in the roll, pitch, and yaw planes, respectively. In addition, $\mathrm{s}_\theta = \sin(\theta)$, $\mathrm{c}_\theta = \cos(\theta)$, $\mathrm{t}_\theta = \tan(\theta)$, and so forth; m is the mass of the projectile; $\vec{I}$ is the inertia matrix of the projectile; g is the gravitational acceleration constant; and $[X, Y, Z]^\mathrm{T}$ and $[L, M, N]^\mathrm{T}$ are the aerodynamic forces and moments acting on the projectile body, respectively.

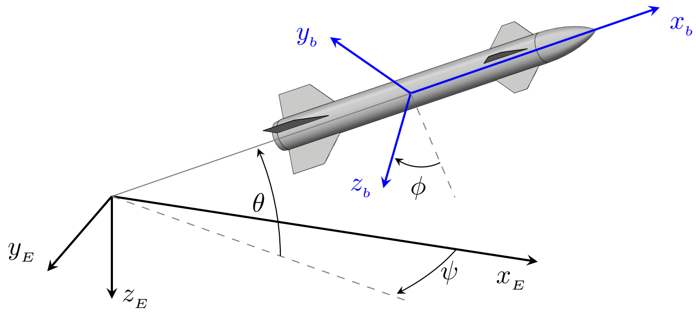

Fig. 1 The body-fixed frame relative to the Earth reference frame (inertial frame)

The aerodynamic forces and moments acting on the projectile body are expressed in the body-fixed frame, whereas the aerodynamic data used to calculate the forces and moments is expressed in the wind frame. The relation between the wind frame and body-fixed frame is depicted in Fig. 2. Using two rotations, a relation between the two frames can be made so the aerodynamic forces and moments calculated in the wind frame can be expressed in the body-fixed frame by

$$\begin{bmatrix} X \\ Y \\ Z \end{bmatrix} = \begin{bmatrix} \mathrm{c}_\alpha \mathrm{c}_\beta & -\mathrm{c}_\alpha \mathrm{s}_\beta & -\mathrm{s}_\alpha \\ \mathrm{s}_\beta & \mathrm{c}_\beta & 0 \\ \mathrm{s}_\alpha \mathrm{c}_\beta & -\mathrm{s}_\alpha \mathrm{s}_\beta & \mathrm{c}_\alpha \end{bmatrix} \begin{bmatrix} X_w \\ Y_w \\ Z_w \end{bmatrix} \tag{5}$$

$$\begin{bmatrix} L \\ M \\ N \end{bmatrix} = \begin{bmatrix} \mathrm{c}_\alpha \mathrm{c}_\beta & -\mathrm{c}_\alpha \mathrm{s}_\beta & -\mathrm{s}_\alpha \\ \mathrm{s}_\beta & \mathrm{c}_\beta & 0 \\ \mathrm{s}_\alpha \mathrm{c}_\beta & -\mathrm{s}_\alpha \mathrm{s}_\beta & \mathrm{c}_\alpha \end{bmatrix} \begin{bmatrix} L_w \\ M_w \\ N_w \end{bmatrix} \tag{6}$$

where $\mathrm{s}_\alpha = \sin(\alpha)$, $\mathrm{c}_\alpha = \cos(\alpha)$, and so forth; and $[X_w, Y_w, Z_w]^\mathrm{T}$ and $[L_w, M_w, N_w]^\mathrm{T}$ are the aerodynamic forces and moments computed in the wind frame, respectively. The aerodynamic forces in the wind frame are referred to as the axial, side, and normal force, respectively, and the aerodynamic moments are referred to as the rolling, pitching, and yawing moment, respectively.

These aerodynamic forces and moments are nonlinear functions that are dependent on the flight conditions of the projectile and can be given as functions of Mach number, aerodynamic angles, body-fixed angular rates, aerodynamic control surface

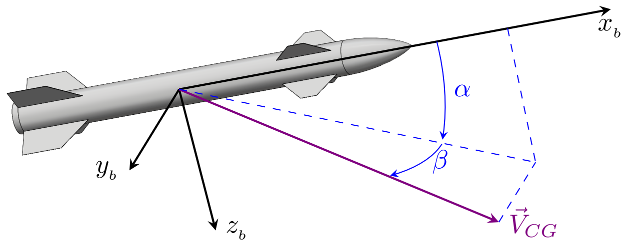

Fig. 2 Wind frame relative to the body-fixed reference frame. Angle of attack and angle of sideslip relate to the projectile's center-of-gravity velocity vector.

deflections, and altitude.[6–9] We express these in functional form as

$$X_w = f\big(\mathrm{M}, \alpha, \beta, \delta_p, h\big), \tag{7}$$

$$Y_w = f\big(\mathrm{M}, \beta, r, \delta_r, h\big), \tag{8}$$

$$Z_w = f\big(\mathrm{M}, \alpha, q, \delta_q, h\big), \tag{9}$$

$$L_w = f\big(\mathrm{M}, \alpha, \beta, p, \delta_p, h\big), \tag{10}$$

$$M_w = f\big(\mathrm{M}, \alpha, q, \delta_q, h\big), \text{ and} \tag{11}$$

$$N_w = f\big(\mathrm{M}, \beta, r, \delta_r, h\big). \tag{12}$$

One can now apply the aerodynamic forces and moments captured from Eqs. 7–12 and related to the appropriate body-fixed frame through Eqs. 5 and 6 to the translational and rotational body-fixed equations of motion in Eqs. 3 and 4, respectively. The result is a nonlinear flight dynamic model of the projectile vehicle that depends on aerodynamic data that varies nonlinearly according to the specific flight condition. For the synthesis and evaluation of gain-scheduled flight controllers, it is advantageous to construct a family of linearized models of the nonlinear flight dynamics that vary across the flight envelope for different flight conditions. This is the reason for using a LPV model to represent the projectile vehicle.

To build these LPV models, we start by modeling the 6DoF equations of motion and the nonlinear aerodynamic forces and moments given by Eqs. 1–12 within Simulink. To account for the variation of aerodynamic data, we use the Committee on Extension to the Standard Atmosphere atmospheric model to provide density and speed of sound versus altitude within the simulation.[10] Once the flight dynamics and aerodynamics are modeled, the next step is to trim the model across the flight envelope. This is discussed in the next section.

4. Model Trimming

Before linearization, the dynamic model is trimmed to match various steady-state operating conditions across the flight envelope. As a first step in this process, the desired flight envelope is defined and a sampled collection of discrete flight conditions contained within the flight envelope is created. For this example, the desired flight envelope, Ξ, for the projectile is defined across M, α, β, and h as

$$\Xi = \left\{ \begin{array}{c} 1.5 \leq \mathrm{M} \leq 3.5 \\ |\alpha| \leq 10^\circ \\ |\beta| \leq 5^\circ \\ 0\ \mathrm{km} \leq h \leq 40\ \mathrm{km} \end{array} \right\} . \tag{13}$$

From the sample points across the discretized flight envelope, a corresponding array of operating point specifications is created using MATLAB `operspec` command. Specify the constraints defining the desired trimmed flight characteristics for each operating point in the array. Then solve for the required control deflections to achieve the desired trimmed flight characteristics using an optimizer. This example uses the MATLAB `findop` command, which packages a nonlinear least-squares optimization into a convenient framework for use with the `operspec` command.

The trim conditions for the model are defined to be the desired quasi-equilibrium conditions at each sample point $\xi = [\alpha, \beta, \mathrm{M}, h] \in \Xi$, as given in Table 1. Equilibrium conditions assume all forces and moments are zero, therefore the trimmed body angular rates, p_0, q_0, r_0, are defined as steady state (but unknown value). For aerospace vehicles with variable thrust as a control input, the trimmed body velocity $[u_0, v_0, w_0]$ can be defined as steady state as well. For projectiles lacking propulsion, however, only quasi-equilibrium conditions have a feasible trim solution (where $F_x \neq 0$), and therefore u_0 is defined as non-steady state. In either case, $[u_0, v_0, w_0]$ are set as known quantities, with values calculated from the stability-axis velocity components $[V_0, \alpha_0, \beta_0]$ at each trim point.

As the body velocity components are nonzero, the $[x_0, y_0, z_0]$ Euler position vector is non-steady state, but known to be $[0, 0, -h]$ for each trim point. The Euler angles $[\phi_0, \theta_0, \psi_0]$ are set to zero and are non-steady at trim (with rates $[p_0, q_0, r_0]$ unknown and steady-state, as previously mentioned).

Table 1 Trim conditions

Parameter	Conditions		
$[x_0, y_0, z_0]$	Non-steady	Known	$[0, 0, -h]$
$[\phi_0, \theta_0, \psi_0]$	Non-steady	Known	$[0, 0, 0]$
u_0	Non-steady[a]	Known	$V_0 \cos(\alpha_0) \cos(\beta_0)$
v_0	Steady state	Known	$V_0 \sin(\beta_0)$
w_0	Steady state	Known	$V_0 \sin(\alpha_0)$
$[p_0, q_0, r_0]$	Steady state	Unknown	

[a] For projectiles lacking thrust

5. Model Linearization

Once the trim conditions have been identified, the linearization process tries to accurately represent the nonlinear flight dynamics and aerodynamics from Eqs. 1–12 in a small region surrounding a trim point by approximating the nonlinear behavior with a linear approximation. Each resulting LTI model takes the form of

$$\begin{aligned} \Delta\dot{\mathbf{x}} &= \mathbf{A}\boldsymbol{\Delta}\mathbf{x} + \mathbf{B}\boldsymbol{\Delta}\mathbf{u}, \\ \Delta\mathbf{y} &= \mathbf{C}\boldsymbol{\Delta}\mathbf{x} + \mathbf{D}\boldsymbol{\Delta}\mathbf{u}, \end{aligned} \tag{14}$$

where Δ indicates perturbations around the trim condition. These individual LTI models are collected into an LPV system where the coefficients of the linear dynamics are dependent on the scheduling parameters represented by

$$\begin{aligned} \Delta\dot{\mathbf{x}} &= \mathbf{A}(\xi)\boldsymbol{\Delta}\mathbf{x} + \mathbf{B}(\xi)\boldsymbol{\Delta}\mathbf{u}, \\ \Delta\mathbf{y} &= \mathbf{C}(\xi)\boldsymbol{\Delta}\mathbf{x} + \mathbf{D}(\xi)\boldsymbol{\Delta}\mathbf{u}, \end{aligned} \tag{15}$$

where ξ is a particular point within the flight envelope, Ξ (given in Eq. 13), and $\mathbf{A}$, $\mathbf{B}$, $\mathbf{C}$, and $\mathbf{D}$ are linear matrices calculated at each ξ. Canonical LPV systems depend on exogenous parameters only; in this case we have a quasi-LPV system which depends both on exogenous parameters as well as the system state. However, for brevity this report will continue to use the term “LPV model.”

Each linear model describes the perturbed system behavior near a quasi-equilibrium trim point; the trim state, input, and output conditions must be included as offsets to the model to fully describe the system. To enable the explicit inclusion of these trim offsets, we use the *affine* form of the LPV model given by

$$\begin{aligned} \Delta\dot{\mathbf{x}} &= \mathbf{A}(\xi)(\mathbf{\Delta x} - \bar{\mathbf{x}}(\xi)) + \mathbf{B}(\xi)(\mathbf{\Delta u} - \bar{\mathbf{u}}(\xi)) + \bar{\dot{\mathbf{x}}}(\xi), \\ \Delta\mathbf{y} &= \mathbf{C}(\xi)(\mathbf{\Delta x} - \bar{\mathbf{x}}(\xi)) + \mathbf{D}(\xi)(\mathbf{\Delta u} - \bar{\mathbf{u}}(\xi)) + \bar{\mathbf{y}}(\xi), \end{aligned} \tag{16}$$

where $\bar{\mathbf{u}}$, $\bar{\mathbf{y}}$, $\bar{\mathbf{x}}$, $\bar{\dot{\mathbf{x}}}$, are the trim offset terms for the inputs, outputs, states, and state derivatives, respectively. Using this formulation, the trim offsets can be packaged together with the LTI array using and used with the MATLAB State-Space Array and Simulink LPV Block to provide accurate simulation of the nonlinear system over the flight envelope. In the remainder of this report, the Δ symbols in the linear models are dropped for brevity.

5.1 6DoF Linear Models

Each LTI model assumes a rigid airframe with symmetry about the body-axis vertical plane of the vehicle[11–13] and describes the location and orientation of the vehicle body with respect to the inertial reference frame.

5.1.1 12-State Body-Fixed Model

One common model formulation combines Cartesian body position, Euler angles, body velocity, and Euler angle rates into a 12-state model, with state vector $[x, y, z, \phi, \theta, \psi, u, v, w, p, q, r]^T$.

A generalized example of this 12-state linear model structure is given in Eq. 17, with expanded terms listed in Table 2.[11,12] In this notation, $_0$ indicates trim value, c and s are cosine and sine functions, respectively, and variable subscripts indicate partial derivatives (e.g., $X_u = \partial X/\partial u$).

$$
\begin{bmatrix} \dot{x} \\ \dot{y} \\ \dot{z} \\ \dot{\phi} \\ \dot{\theta} \\ \dot{\psi} \\ \dot{u} \\ \dot{v} \\ \dot{w} \\ \dot{p} \\ \dot{q} \\ \dot{r} \end{bmatrix}
=
\begin{bmatrix}
0 & 0 & 0 & 0 & \overline{uw}_1 & \overline{uw}_4 & c_{\theta_0} & 0 & s_{\theta_0} & 0 & 0 & 0 \\
0 & 0 & 0 & w_0 & 0 & \overline{uw}_2 & 0 & 1 & 0 & 0 & 0 & 0 \\
0 & 0 & 0 & v_0 & \overline{uw}_3 & 0 & -s_{\theta_0} & 0 & c_{\theta_0} & 0 & 0 & 0 \\
0 & 0 & 0 & 0 & 0 & 0 & 0 & 0 & 0 & 1 & 0 & \tan\theta_0 \\
0 & 0 & 0 & 0 & 0 & 0 & 0 & 0 & 0 & 0 & 1 & 0 \\
0 & 0 & 0 & 0 & 0 & 0 & 0 & 0 & 0 & 0 & 0 & \sec\theta_0 \\
0 & 0 & X_z & 0 & -gc_{\theta_0} & 0 & X_u & X_v & X_w & 0 & (X_q - w_0) & (X_r - v0) \\
0 & 0 & 0 & gc_{\theta_0} & 0 & 0 & 0 & Y_v & Y_w & (Y_p + w_0) & 0 & (Y_r - u_0) \\
0 & 0 & \frac{Z_z}{(1-Z_{\dot{w}})} & 0 & -gs_{\theta_0} & 0 & \frac{Z_u}{(1-Z_{\dot{w}})} & \frac{Z_v}{(1-Z_{\dot{w}})} & \frac{Z_w}{(1-Z_{\dot{w}})} & \frac{Z_p - v_0}{(1-Z_{\dot{w}})} & \frac{Z_q + u_0}{(1-Z_{\dot{w}})} & 0 \\
0 & 0 & 0 & L_\phi & 0 & 0 & 0 & L_v & L_w & L_p & 0 & L_r \\
0 & 0 & 0 & 0 & \overline{M}_\theta & 0 & \overline{M}_u & \overline{M}_v & \overline{M}_w & \overline{M}_p & \overline{M}_q & 0 \\
0 & 0 & 0 & N_\phi & 0 & 0 & \overline{N}_u & \overline{N}_v & \overline{N}_w & \overline{N}_p & 0 & \overline{N}_r
\end{bmatrix}
\begin{bmatrix} x \\ y \\ z \\ \phi \\ \theta \\ \psi \\ u \\ v \\ w \\ p \\ q \\ r \end{bmatrix}
+
\begin{bmatrix}
\multicolumn{4}{c}{0_{6\times 4}} \\
X_{\delta_p} & X_{\delta_q} & X_{\delta_r} & X_{\delta_T} \\
Y_{\delta_p} & Y_{\delta_q} & Y_{\delta_r} & Y_{\delta_T} \\
\overline{Z}_{\delta_p} & \overline{Z}_{\delta_q} & \overline{Z}_{\delta_r} & \overline{Z}_{\delta_T} \\
L_{\delta_p} & L_{\delta_q} & L_{\delta_r} & L_{\delta_T} \\
\overline{M}_{\delta_p} & \overline{M}_{\delta_q} & \overline{M}_{\delta_r} & \overline{M}_{\delta_T} \\
\overline{N}_{\delta_p} & \overline{N}_{\delta_q} & \overline{N}_{\delta_r} & \overline{N}_{\delta_T}
\end{bmatrix}
\begin{bmatrix} \delta_p \\ \delta_q \\ \delta_r \\ \delta_T \end{bmatrix}
\tag{17}
$$

Table 2 Expanded terms from 12-state linear model

$\overline{uw}_1$	$= -u_0 s_{\theta_0} + w_0 c_{\theta_0}$		
$\overline{uw}_2$	$= u_0 c_{\theta_0} + w_0 s_{\theta_0}$	$\overline{Z}_{\delta_p}$	$= \frac{Z_{\delta_p}}{(1-Z_{\dot{w}})}$
$\overline{uw}_3$	$= -u_0 c_{\theta_0} - w_0 s_{\theta_0}$	$\overline{Z}_{\delta_q}$	$= \frac{Z_{\delta_q}}{(1-Z_{\dot{w}})}$
$\overline{uw}_4$	$= u_0 s_{\theta_0} + v_0 s_{\theta_0}$	$\overline{Z}_{\delta_r}$	$= \frac{Z_{\delta_r}}{(1-Z_{\dot{w}})}$
$\overline{M}_\theta$	$= M_\theta + \frac{M_{\dot{w}} g \sin\theta_0}{(1-Z_{\dot{w}})}$	$\overline{Z}_{\delta_T}$	$= \frac{Z_{\delta_T}}{(1-Z_{\dot{w}})}$
$\overline{M}_u$	$= M_u + \frac{M_{\dot{w}} Z_u}{(1-Z_{\dot{w}})}$	$\overline{M}_{\delta_p}$	$= M_{\delta_p} + \frac{M_{\dot{w}} Z_{\delta_p}}{(1-Z_{\dot{w}})}$
$\overline{M}_v$	$= M_v + \frac{M_{\dot{w}} Z_v}{(1-Z_{\dot{w}})}$	$\overline{M}_{\delta_q}$	$= M_{\delta_q} + \frac{M_{\dot{w}} Z_{\delta_q}}{(1-Z_{\dot{w}})}$
$\overline{M}_w$	$= M_w + \frac{M_{\dot{w}} Z_w}{(1-Z_{\dot{w}})}$	$\overline{M}_{\delta_r}$	$= M_{\delta_r} + \frac{M_{\dot{w}} Z_{\delta_r}}{(1-Z_{\dot{w}})}$
$\overline{M}_p$	$= M_p + \frac{M_{\dot{w}}(Z_p+u_0)}{(1-Z_{\dot{w}})}$	$\overline{M}_{\delta_T}$	$= M_{\delta_T} + \frac{M_{\dot{w}} Z_{\delta_T}}{(1-Z_{\dot{w}})}$
$\overline{M}_q$	$= M_q + \frac{M_{\dot{w}}(Z_q+u_0)}{(1-Z_{\dot{w}})}$	$\overline{N}_{\delta_p}$	$= N_{\delta_p} + N_{\dot{v}} Y_{\delta_p}$
$\overline{N}_u$	$= N_u + N_{\dot{v}} Y_u$	$\overline{N}_{\delta_q}$	$= N_{\delta_q} + N_{\dot{v}} Y_{\delta_q}$
$\overline{N}_v$	$= N_v + N_{\dot{v}} Y_v$	$\overline{N}_{\delta_r}$	$= N_{\delta_r} + N_{\dot{v}} Y_{\delta_r}$
$\overline{N}_w$	$= N_w + N_{\dot{v}} Y_w$	$\overline{N}_{\delta_T}$	$= N_{\delta_T} + N_{\dot{v}} Y_{\delta_T}$
$\overline{N}_p$	$= N_p + N_{\dot{v}}(Y_p + w_0)$		
$\overline{N}_r$	$= N_r + N_{\dot{v}}(Y_r - u_0)$		

The X_q, Y_p, Y_r, Z_p, Z_q and $Z_{\dot{w}}$ terms are typically small and are often neglected in practice due to their minor influence on the vehicle response.[12]

5.1.2 8-State Stability-Frame Model

Often it is convenient to express the vehicle translational dynamics in the stability-axis (as opposed to the body-axis coordinates used up to this point), and exchange the Cartesian body-frame velocity $[u, v, w]$ for a polar representation $[V, \alpha, \beta]$ within the state vector.[11,12] Assuming small α and β angles, this change can be made according to Table 3.

Table 3 Conversion from body-axis to stability-axis

ΔV	$= \Delta u$	M_α	$= u_0 M_w$
$\Delta \dot{V}$	$= \Delta \dot{u}$	$M_{\dot{\alpha}}$	$= u_0 M_{\dot{w}}$
$\Delta\alpha$	$= \Delta w / u_0$	Z_α	$= u_0 Z_w$
$\Delta\dot{\alpha}$	$= \Delta\dot{w} / u_0$	N_β	$= u_0 N_v$
$\Delta\beta$	$= \Delta v / u_0$	$N_{\dot{\beta}}$	$= u_0 N_{\dot{v}}$
$\Delta\dot{\beta}$	$= \Delta\dot{v} / u_0$	Y_β	$= u_0 Y_v$

Additionally, the $x, y, z,$ and ψ states can be neglected for compactness, depending on the application. These changes result in Eq. 18, which is a typical dynamic model formulation for flight control design.

$$
\begin{bmatrix} \dot{V} \\ \dot{\phi} \\ \dot{\theta} \\ \dot{\alpha} \\ \dot{\beta} \\ \dot{p} \\ \dot{q} \\ \dot{r} \end{bmatrix}
=
\begin{bmatrix}
X_V & 0 & -gc_{\theta_0} & X_\alpha & X_\beta & 0 & -w_0 & v_0 \\
0 & 0 & 0 & 0 & 0 & 1 & 0 & \tan\theta_0 \\
0 & 0 & 0 & 0 & 0 & 0 & 1 & 0 \\
Z_V/u_0 & 0 & -gs_{\theta_0}/u_0 & Z_\alpha/u_0 & Z_\beta/u_0 & -v_0/u_0 & 1 & 0 \\
0 & gc_{\theta_0}/u_0 & 0 & Y_\alpha/u_0 & Y_\beta/u_0 & w_0/u_0 & 0 & -1 \\
0 & L_\phi & 0 & L_\alpha & L_\beta & L_p & 0 & L_r \\
M_V & 0 & M_\theta & M_\alpha + M_{\dot{\alpha}}\frac{Z_\alpha}{u_0} & M_\beta + M_{\dot{\alpha}}\frac{Z_\beta}{u_0} & 0 & M_q + M_{\dot{\alpha}} & 0 \\
0 & N_\phi & 0 & N_\alpha + N_{\dot{\beta}}\frac{Y_\alpha}{u_0} & N_\beta + N_{\dot{\beta}}\frac{Y_\beta}{u_0} & N_p + N_{\dot{\beta}}\frac{w_0}{u_0} & 0 & N_r - N_{\dot{\beta}}
\end{bmatrix}
\begin{bmatrix} V \\ \phi \\ \theta \\ \alpha \\ \beta \\ p \\ q \\ r \end{bmatrix}
+
\begin{bmatrix}
X_{\delta_p} & X_{\delta_q} & X_{\delta_r} & X_{\delta_T} \\
0 & 0 & 0 & 0 \\
0 & 0 & 0 & 0 \\
0 & Z_{\delta_q}/u_0 & 0 & 0 \\
Y_{\delta_p}/u_0 & 0 & Y_{\delta_r}/u_0 & 0 \\
L_{\delta_p} & L_{\delta_q} & L_{\delta_r} & L_{\delta_T} \\
M_{\delta_p} & M_{\delta_q} & M_{\delta_r} & M_{\delta_T} \\
N_{\delta_p} & N_{\delta_q} & N_{\delta_r} & N_{\delta_T}
\end{bmatrix}
\begin{bmatrix} \delta_p \\ \delta_q \\ \delta_r \\ \delta_T \end{bmatrix}
\tag{18}
$$

5.1.3 Numerical Example

A sample linear model is populated for a $[\mathrm{M} = 2, \alpha = 5°, \beta = 0°, h = 0 \text{ km}]$ flight condition with no thrust, following the form of Eq. 18. The trim conditions for this example are given in Table 4, and the corresponding trim offset terms for the inputs, states, and state derivatives are given in Table 5. The resulting linear model is given by Eq. 19. An equivalent linear model and set of offsets following the body-frame, 12-state model formulation of Eq. 17 is included in the Appendix for reference.

Table 4 Trim condition for numerical example

V_0	=	680 m/s
$[\alpha_0, \beta_0]$	=	$[5^o, 0^o]$
$[x_0, y_0, z_0]$	=	$[0, 0, 0]$
$[\phi_0, \theta_0, \psi_0]$	=	$[0, 0, 0]$
u_0	=	677.9 m/s
v_0	=	0 m/s
w_0	=	59.4 m/s

Table 5 Offsets for linear model example

States	Derivatives	Inputs
$\overline{V}$ = 677.99	$\dot{\overline{V}}$ = -123.44	$\overline{\delta}_p$ = 0.003
$\overline{\phi}$ = 0	$\dot{\overline{\phi}}$ = 0	$\overline{\delta}_q$ = 3.7667
$\overline{\theta}$ = 0	$\dot{\overline{\theta}}$ = 1.1983	$\overline{\delta}_r$ = -0.00045
$\overline{\alpha}$ = 0.087625	$\dot{\overline{\alpha}}$ = 1.0664	
$\overline{\beta}$ = 0	$\dot{\overline{\beta}}$ = 0.0097333	
$\overline{p}$ = 0	$\dot{\overline{p}}$ = 0	
$\overline{q}$ = 1.1983	$\dot{\overline{q}}$ = 0	
$\overline{r}$ = -0.0109	$\dot{\overline{r}}$ = 0	

$$
\begin{bmatrix} \dot{V} \\ \dot{\phi} \\ \dot{\theta} \\ \dot{\alpha} \\ \dot{\beta} \\ \dot{p} \\ \dot{q} \\ \dot{r} \end{bmatrix} = \begin{bmatrix} -0.113 & 0 & -9.798 & -1.2075 & -0.011 & 0 & -59.41 & 0 \\ 0 & 0 & 0 & 0 & 0 & 1 & 0 & 0 \\ 0 & 0 & 0 & 0 & 0 & 0 & 1 & 0 \\ 0.0016 & 0 & 0 & -2.193 & 0 & 0 & 1 & 0 \\ 0 & 0.0145 & 0 & 0 & -2.277 & 0.088 & 0 & -1 \\ 0 & 0 & 0 & 0 & 476.68 & -2.66 & 0 & 0 \\ 0.0739 & 0 & 0 & -1174.1 & 0 & 0 & -2.796 & 0 \\ 0 & 0 & 0 & 0 & 1256.9 & -1.177 & 0 & -2.796 \end{bmatrix} \begin{bmatrix} V \\ \phi \\ \theta \\ \alpha \\ \beta \\ p \\ q \\ r \end{bmatrix}
+ \begin{bmatrix} 0 & -1.8952 & 0 \\ 0 & 0 & 0 \\ 0 & 0 & 0 \\ 0 & 0.0047 & 0 \\ -0.0004 & 0 & -0.0048 \\ 236.6161 & 0 & 10.6299 \\ 0 & 15.5220 & 0 \\ 2.3209 & 0 & 15.8657 \end{bmatrix} \begin{bmatrix} \delta_p \\ \delta_q \\ \delta_r \end{bmatrix} \tag{19}
$$

5.2 Eigenvalue and Modal Analysis

An analysis of the 6DoF linear model is performed to identify the modes of motion representing the dominant dynamic behaviors and which states are the key contributors to each mode. This technique is useful in simplifying large, complex LTI dynamic models into more compact representations. The eigenvalues of the linear model state transition matrix given in Eq. 19 are provided in Table 6.

Table 6 Eigenvalues for linear model example

λ_1, λ_2	$=$	-2.7726	$\pm 34.86i$
λ_3, λ_4	$=$	-2.5371	$\pm 34.331i$
λ_5	$=$	-2.1958	$+0i$
λ_6	$=$	0.00717	$+0i$
λ_7	$=$	-0.13359	$+0i$
λ_8	$=$	0.10557	$+0i$

This model can be analyzed using a sensitivity matrix, S, that identifies the effect of small changes in each state on the eigenvalues. Using this tool, the driving states corresponding to each dynamic mode can be identified, and the dynamic system can be decoupled into smaller models using superposition.[11,14]

The sensitivity matrix for the linear model state transition matrix given in Eq. 19 is provided in Table 7, with the dominant terms for each eigenvalue highlighted. The states which most heavily influence each flight mode can then be identified.

1. **Dutch-Roll** (λ_1, λ_2): dominated by β and r for this example case with a symmetric flight vehicle; asymmetric vehicles can also have significant contributions from p and phi as the lateral-directional coupling increases.

2. **Short-Period** (λ_3, λ_4): dominated by α and q.

3. **Rolling** λ_5: dominated by p in this case; with asymmetric vehicles this mode can have contributions from ϕ and/or β as well.

4. **Spiral** λ_6: dominated by ϕ.

5. **Phugoid** (λ_7, λ_8): dominated by V and θ.

Using the results from the sensitivity matrix, it is clear that the different dynamic modes are uncoupled and the model can be separated into smaller models that each capture a subset of the overall behavior. The *longitudinal dynamics* corresponding to the short period and phugoid modes can be expressed in a model with states $[V, \theta, \alpha, q]^T$ (optionally including x, z). The *lateral dynamics* are often tightly coupled with the *directional dynamics*, so are typically left as coupled *lateral-directional dynamics* corresponding to the Dutch-roll, rolling, and spiral modes that can be expressed in a model with states $[\phi, \beta, p, r]^T$ (optionally including y, ψ).

Table 7 Sensitivity matrix for linear model example (stability-axis)

	λ_1, λ_2 -2.7726 $\pm$ 34.86i		λ_3, λ_4 -2.5371 $\pm$ 34.331i		λ_5 -2.196 + 0i	λ_6 0.00717 + 0i	λ_7 -0.1336 + 0i	λ_8 0.1056 + 0i
V	1.4076e-24	1.4076e-24	0.0023	0.0023	1.3853e-35	3.7030e-29	**0.5563**	**0.4396**
ϕ	8.0782e-05	8.0782e-05	1.1927e-24	1.1927e-24	7.0315e-04	**0.9993**	2.5008e-22	3.8097e-22
θ	1.5190e-25	1.5190e-25	1.1077e-05	1.1077e-05	7.8301e-26	6.3087e-22	**0.4442**	**0.5558**
α	3.7071e-23	3.7071e-23	**0.4981**	**0.4981**	3.7101e-27	1.1137e-25	5.1129e-04	0.0044
β	**0.4999**	**0.4999**	3.8150e-23	3.8150e-23	2.2880e-04	1.9910e-05	2.5991e-26	3.9125e-26
p	0.0184	0.0184	1.4589e-24	1.4589e-24	**1.0307**	0.0034	2.2435e-24	3.6807e-24
q	3.7942e-23	3.7942e-23	**0.4999**	**0.4999**	1.9935e-27	5.2178e-26	1.8863e-05	1.8798e-04
r	**0.5171**	**0.5171**	4.0739e-23	4.0739e-23	0.0316	0.0027	1.3421e-23	1.4798e-23

Bold numbers indicate dominant terms

Figure 3 plots eigenvalues for the example case, with the eigenvalues corresponding to the dominant flight modes labeled on the figure. Following the results of the modal analysis from Table 7, the decoupled longitudinal and lateral-directional model eigenvalues are provided along with the 6DoF body-frame and stability-frame formulations. The details of these decoupled dynamics models are presented in Sections 5.3 and 5.4.

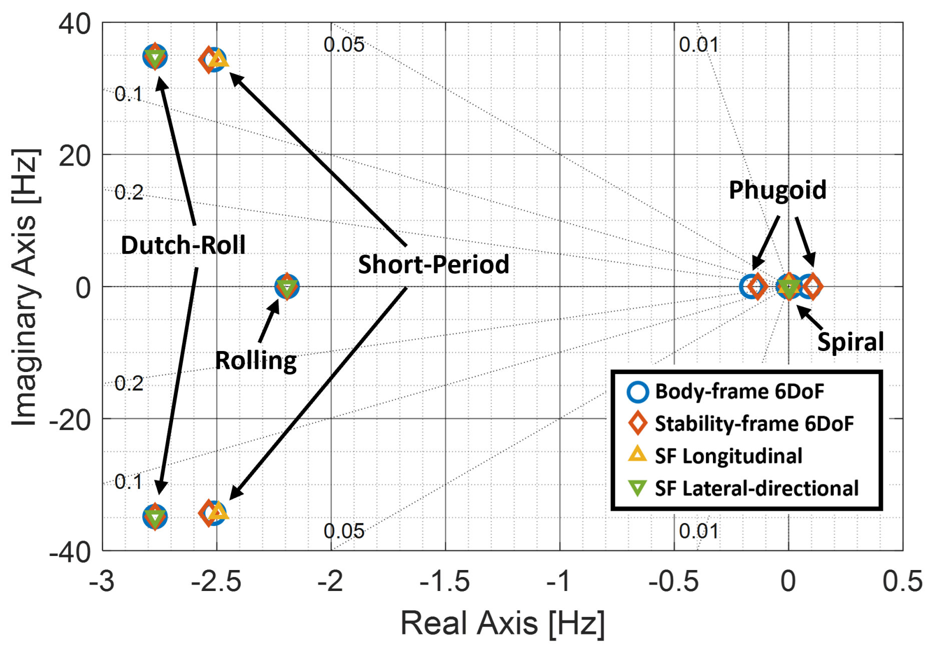

Fig. 3 Eigenvalues for example case

5.3 Longitudinal Dynamics Models

The model describing the 3DoF longitudinal (pitch-plane) dynamics contains the phugoid and short-period modes and is written as

$$\begin{bmatrix} \dot{V} \\ \dot{\theta} \\ \dot{\alpha} \\ \dot{q} \end{bmatrix} = \begin{bmatrix} X_V & -gc_{\theta_0} & X_\alpha & -w_0 \\ 0 & 0 & 0 & 1 \\ Z_V/u_0 & -gs_{\theta_0}/u_0 & Z_\alpha/u_0 & 1 \\ M_V & M_\theta & M_\alpha + M_{\dot{\alpha}}\frac{Z_\alpha}{u_0} & M_q + M_{\dot{\alpha}} \end{bmatrix} \begin{bmatrix} V \\ \theta \\ \alpha \\ q \end{bmatrix} + \begin{bmatrix} X_{\delta_q} & X_{\delta_T} \\ 0 & 0 \\ Z_{\delta_q}/u_0 & Z_{\delta_T}/u_0 \\ M_{\delta_q} & M_{\delta_T} \end{bmatrix} \begin{bmatrix} \delta_q \\ \delta_T \end{bmatrix}. \tag{20}$$

For some use cases, the longitudinal dynamics model from Eq. 20 is often simplified further to focus on the faster short-period mode, as shown in Eq. 21. This model assumes $\Delta u = 0$ and neglects phugoid mode dynamics. For symmetric projectiles at low angles of attack, this can also be used as a model for the yaw-plane dynamics with appropriate sign and variable changes.

$$\begin{aligned}\begin{bmatrix} \dot{\alpha} \\ \dot{q} \end{bmatrix} &= \begin{bmatrix} Z_\alpha/u_0 & 1 \\ M_\alpha + M_{\dot{\alpha}}\frac{Z_\alpha}{u_0} & M_q + M_{\dot{\alpha}} \end{bmatrix} \begin{bmatrix} \alpha \\ q \end{bmatrix} \\ &+ \begin{bmatrix} Z_{\delta_q}/u_0 & Z_{\delta_T}/u_0 \\ M_{\delta_q} & M_{\delta_T} \end{bmatrix} \begin{bmatrix} \delta_q \\ \delta_T \end{bmatrix}\end{aligned} \tag{21}$$

5.4 Lateral-Directional Dynamics Models

A typical model describing the lateral-directional dynamics drops states y and ψ to focus on the Dutch-roll, spiral, and rolling modes and is written as

$$\begin{aligned}\begin{bmatrix} \dot{\phi} \\ \dot{\beta} \\ \dot{p} \\ \dot{r} \end{bmatrix} &= \begin{bmatrix} 0 & 0 & 1 & \tan\theta_0 \\ gc\theta_0/u_0 & Y_\beta/u_0 & w_0/u_0 & -1 \\ L_\phi & L_\beta & L_p & L_r \\ N_\phi & N_\beta + N_{\dot{\beta}}\frac{Y_\beta}{u_0} & N_p + N_{\dot{\beta}}\frac{w_0}{u_0} & N_r - N_{\dot{\beta}} \end{bmatrix} \begin{bmatrix} \phi \\ \beta \\ p \\ r \end{bmatrix} \\ &+ \begin{bmatrix} 0 & 0 \\ Y_{\delta_p}/u_0 & Y_{\delta_r}/u_0 \\ L_{\delta_p} & L_{\delta_r} \\ N_{\delta_p} & N_{\delta_r} \end{bmatrix} \begin{bmatrix} \delta_p \\ \delta_r \end{bmatrix}.\end{aligned} \tag{22}$$

To build a roll-controller or simulate the roll dynamics alone, the roll states can be taken from Eq. 22 to leave a simple two-state integrator model given in Eq. 23 if supported by the modal analysis.

$$\begin{bmatrix} \dot{\phi} \\ \dot{p} \end{bmatrix} = \begin{bmatrix} 0 & 1 \\ L_\phi & L_p \end{bmatrix} \begin{bmatrix} \phi \\ p \end{bmatrix} + \begin{bmatrix} 0 \\ L_{\delta_p} \end{bmatrix} \delta_p \tag{23}$$

6. LPV Model Validation

This section presents a comparison of the LPV models with the nonlinear 6DoF models to provide a qualitative comparison. Simulink simulations are used to compare the various models side-by-side to demonstrate the relevant dynamics are still captured by the simpler LPV model formulations. All simulations are performed at standard atmosphere, sea level ($h = 0$ km), but the results are similar at other altitudes in the flight envelope.

The simulation results in this section are plotted according to the following color scheme:

- The full nonlinear 6DoF model is shown in black (▬▬),
- The 12-state body-frame 6DoF LPV model described in Section 5.1.1 is shown in blue (▬▬),
- The 8-state 6DoF stability-frame model described in Section 5.1.2 is shown in red (▬▬),
- The decoupled LPV models for short-period longitudinal dynamics (Section 5.3) and lateral-directional dynamics (Section 5.4) are both shown in dashed orange (- - - - -),
- Finally, an LTI model corresponding to the starting trim conditions (e.g., $\mathrm{M} = 2.5$, $\alpha = 5°$, $\beta = 0°$) is included for comparison and shown in green (▬▬).

The simulation results for a simple roll test are shown in Fig. 4. Each model is initialized to a trim condition of $\mathrm{M} = 2.5$, $\alpha = 0°$, and $\beta = 0°$, with an initial perturbation of $p_0 = 3$ rad/s. In this case, the nonlinearities within α and β are not excited, thus models all compare favorably to the nonlinear simulation and are able to accurately predict the response. The LTI model begins to drift away slightly at the end of the simulation as M slows down from 2.5 to 2.0 (not shown).

Figure 5 compares short-period longitudinal motion between the nonlinear 6DoF and relevant LPV formulations. Each simulation is initialized at a trim condition of $\mathrm{M} = 2.5$, $\alpha = 5°$, and $\beta = 0°$, with an initial perturbation of $q_0 = 3$ rad/s. All three LPV models compare very well with the nonlinear 6DoF results in this case. The LTI model shows similar frequency and amplitude, but does not have the same changes with α and so does not match nearly as well.

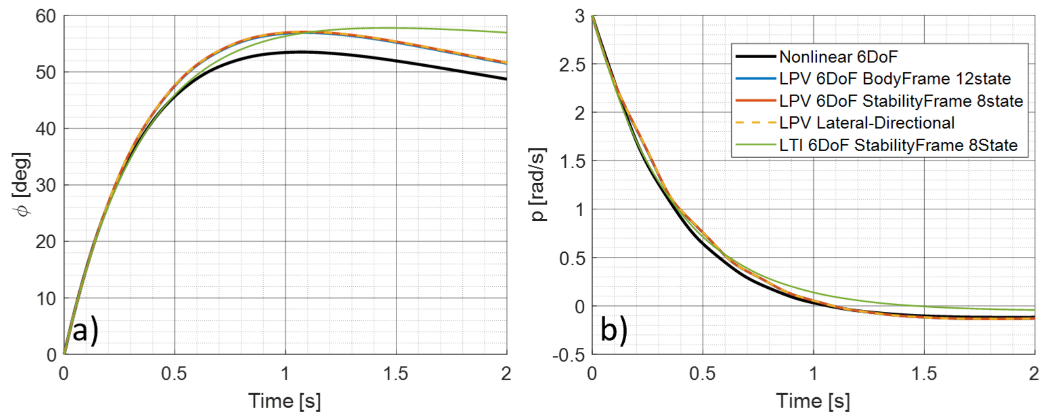

Fig. 4 Comparison of roll dynamics between models

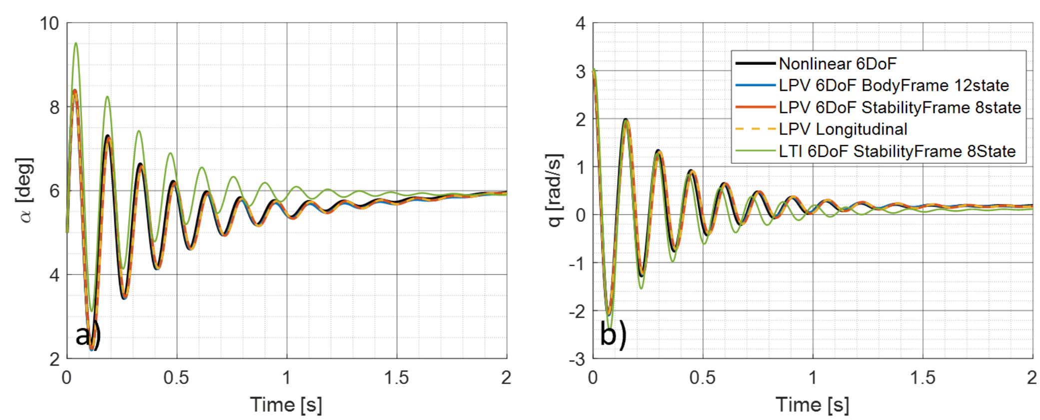

Fig. 5 Comparison of short-period dynamics between models

Figure 6 compares lateral-directional motion between the models. Each simulation is initialized at $\mathrm{M} = 2.5$, $\alpha = 0°$, and $\beta = 3°$ and perterbed in both roll and yaw by $p_0 = 3$ rad/s and $r_0 = 3$ rad/s. All LPV models compare very well to the nonlinear 6DoF results in β and r. The LPV model response in p is reasonably close, but slightly underpredicts the induced roll rate and shows more oscillations than are given by the nonlinear results. The LTI model lacking the scheduled parameters across β does not match the true behavior well in either yaw or roll.

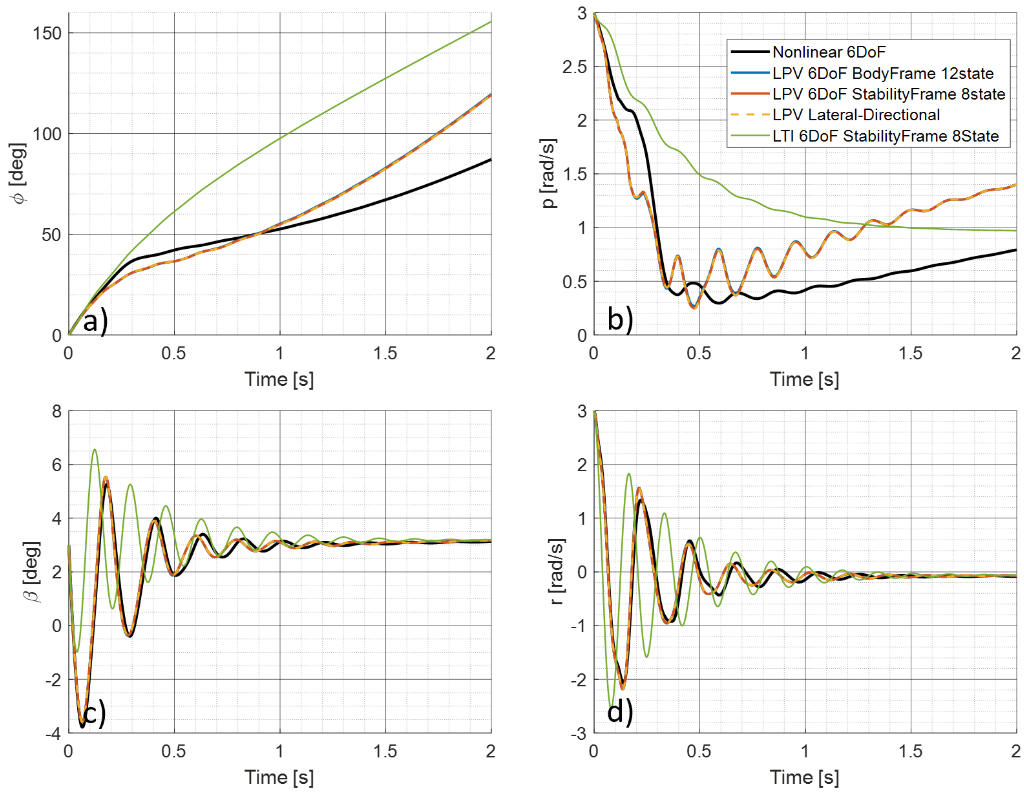

Fig. 6 Comparison of lateral-directional dynamics between models

Figure 7 compares full 6DoF motion between the models. Each simulation is initialized at $\mathrm{M} = 2.5$, $\alpha = 5°$, and $\beta = 3°$ and perturbed in roll, pitch, and yaw by $p_0 = 3$ rad/s, $q_0 = 3$ rad/s, and $r_0 = 3$ rad/s. All LPV models compare well to the nonlinear 6DoF results. The LTI model, lacking the scheduled parameters across α and β, is a poorer predictor of the true behavior.

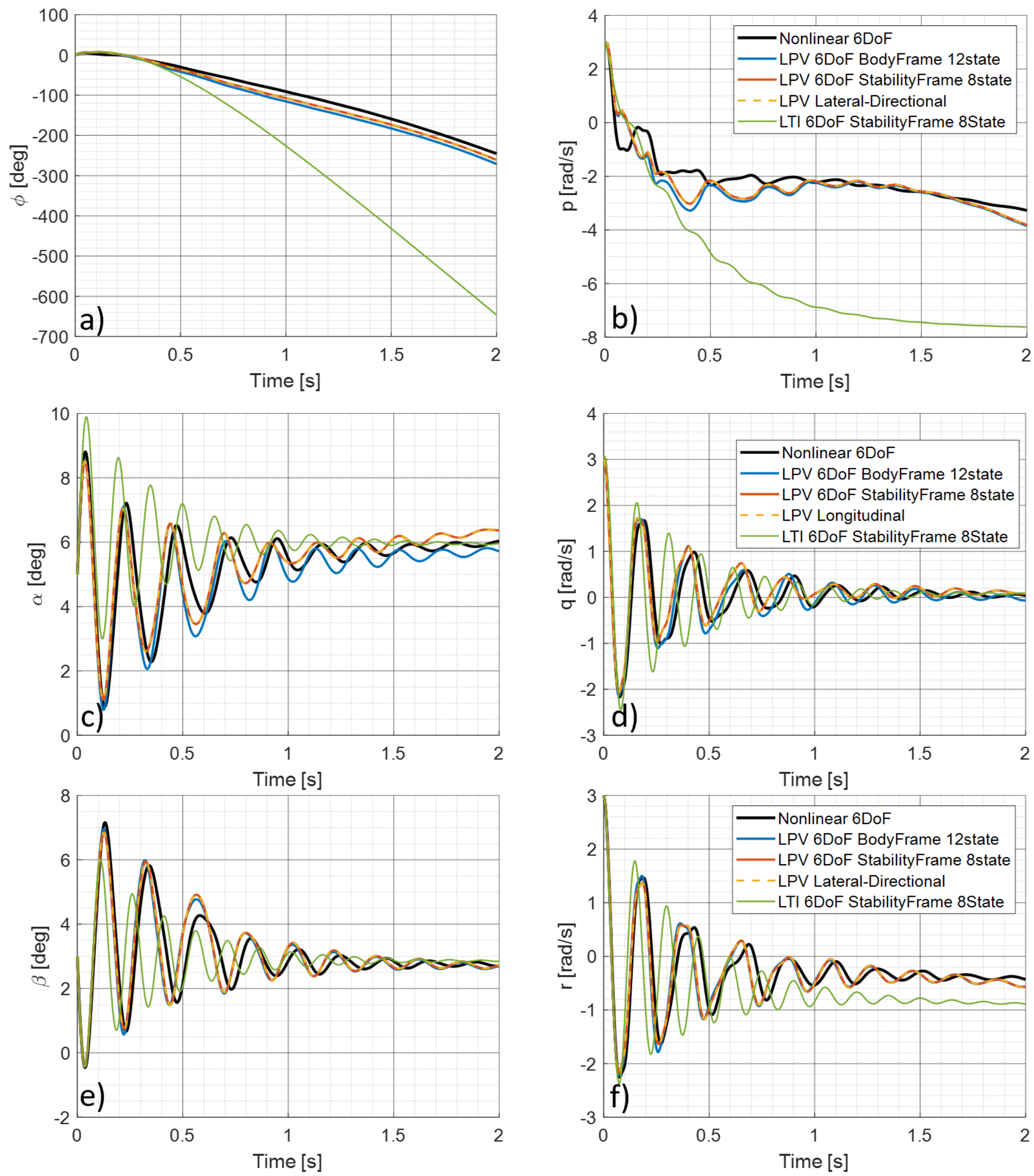

Fig. 7 Comparison of 6DoF dynamics between models

7. Conclusion

This report presented the LPV model formulation for representing vehicle dynamics across a wide flight envelope. This approach has advantages in the design of gain-scheduled controllers and provides a more convenient and compact method of sharing models between research groups.

An example nonlinear model was described briefly and the process for trimming and linearizing a nonlinear model was presented. Several linear models typically used to represent the dynamics of aerospace vehicles were discussed, and a method to identify the dominant modes of motion was presented. The collection of LTI models across a flight envelope were gathered into an LPV model formulation along with the associated trim conditions. These LPV models were validated against the full nonlinear model in simulation.

However, this LPV approach based on LTI models does not capture the transient behaviors between model sample points or flight in non-trim conditions, potentially neglecting important nonlinearities and coupling terms that can affect the system behavior. Future work will explore the State Transformation method used to provide an exact transformation between the original nonlinear system and an associated LPV model to avoid these approximation errors. This approach generates an LPV model which is independent of any specific operating point and accounts for off-trim conditions.

8. References

1. Bryson J, Gruenwald BC. Automated gain-scheduling approach for three-loop autopilot. DEVCOM Army Research Laboratory (US); 2022 Sep. Report No.: ARL-TR-9564.

2. Griffith TD, Zelina J, Bryson JT, Gruenwald BC. Dynamic inversion with adaptive augmentation for a high-speed guided projectile. DEVCOM Army Research Laboratory (US); 2022 Dec. Report No.: ARL-TR-9620.

3. Bryson J, Gruenwald BC. Linear parameter varying model predictive control of a high-speed projectile. AIAA Scitech 2022 Forum; 2022 Jan. Paper No.: AIAA 2022-1585.

4. Vinco GM, Theodoulis S, Sename O, Strub G. Linear parameter varying pitch autopilot design for a class of long range guided projectiles. AIAA Scitech 2023 Forum; 2023 Jan. Paper No.: AIAA 2023-2498.

5. Vinco G, Theodoulis S, Sename O, Strub G. Quasi-lpv modeling of guided projectile pitch dynamics through state transformation technique. IFAC-PapersOnLine. 2022;55(35):43–48.

6. Vasile J, Sahu J. Roll orientation–dependent aerodynamics of a long-range projectile. DEVCOM Army Research Laboratory (US); 2020 Aug. Report No.: ARL-TR-9017.

7. Vasile JD, Bryson JT, Sahu J, Paul JL, Gruenwald BC. Aerodynamic dataset generation of a long-range projectile. DEVCOM Army Research Laboratory (US); 2020 Aug. Report No.: ARL-TR-9019.

8. Burchett BT, Vasile JD, Bryson J. Combining sparse and dense databases to form a robust aerodynamic model for a long-range, high-speed projectile. AIAA Scitech 2022 Forum; 2022 Jan. Paper No.: AIAA 2022-0419.

9. Bryson J, Vasile JD, Gruenwald BC, Saju J, Fresconi F. Modeling and flight dynamics of a projectile with nonlinear, roll-dependent aerodynamics. AIAA Scitech 2021 Forum; 2021 Jan. Paper No.: AIAA 2021-0823.

10. National Oceanic and Atmospheric Administration, National Aeronautics and Space Administration, and United States Air Force. U.S. Standard Atmosphere, 1976. 1977 Feb. Report No.: ADA035728.

11. Stengel RF. Flight dynamics. 2nd edition. Princeton University Press; 2022.

12. Nelson RC. Flight stability and automatic control. 2nd edition. McGraw Hill; 1998.

13. Yechout TR. Introduction to aircraft flight mechanics. 2nd edition. American Institute of Aeronautics and Astronautics, Inc.; 2014.

14. Wiese DP. Adaptive control of a generic hypersonic vehicle. Massachusetts Institute of Technology; 2013.

Appendix. Sample Linear Model

A sample linear model is populated for a $[\mathrm{M}=2, \alpha=5°, \beta=0°, h=0\ \mathrm{km}]$ flight condition, following the form of Eq. 18 in the main report. The trim offsets are given in Table A-1 and the linear model terms are given in Eq. A-1.

Table A-1 Offsets for linear model example

States		State derivatives		Inputs	
x	0	x	677.9902	dp	0.0030
y	0	y	0.0108	dq	3.7667
z	0	z	59.4246	dr	-4.4799e-04
ϕ	0	ϕ	8.2044e-09	0	0
θ	-2.2990e-05	θ	1.1983	0	0
ψ	0	ψ	-0.0109	0	0
u	677.9916	u	-123.4416	0	0
v	0.0108	v	6.5991	0	0
w	59.4090	w	723.0124	0	0
p	-2.4201e-07	p	1.1071e-11	0	0
q	1.1983	q	1.7333e-09	0	0
r	-0.0109	r	-9.6794e-10	0	0

The eigenvalues of the linear model state transition matrix given in Eq. A-1 are provided in Table A-2. The four repeated eigenvalues at the origin correspond to the state dynamics in x, y, z, and ψ; these are removed in subsequent analyses for compactness. The remaining eight states are $[\phi, \theta, u, v, w, p, q, r]^T$. The resulting sensitivity matrix for this eight state linear model is provided in Table A-3.

Table A-2 Eigenvalues for 12-state linear model example

λ_1, λ_2	$=$	-2.7726	$\pm 34.86i$
λ_3, λ_4	$=$	-2.5102	$\pm 34.348i$
λ_5	$=$	-2.1958	$+0i$
λ_6	$=$	0.00717	$+0i$
λ_7	$=$	-0.1666	$+0i$
λ_8	$=$	0.0846	$+0i$
$\lambda_9 : \lambda_{12}$	$=$	0	$+0i$

$$
\begin{bmatrix} \dot{x} \\ \dot{y} \\ \dot{z} \\ \dot{\phi} \\ \dot{\theta} \\ \dot{\psi} \\ \dot{u} \\ \dot{v} \\ \dot{w} \\ \dot{p} \\ \dot{q} \\ \dot{r} \end{bmatrix}
=
\begin{bmatrix}
0 & 0 & 0 & 0 & 59.4 & 0 & 1 & 0 & 0 & 0 & 0 & 0 \\
0 & 0 & 0 & -59.4 & 0 & 677.9 & 0 & 1 & 0 & 0 & 0 & 0 \\
0 & 0 & 0 & 0 & -677.9 & 0 & 0 & 0 & 1 & 0 & 0 & 0 \\
0 & 0 & 0 & 0 & 0 & 0 & 0 & 0 & 0 & 1 & 0 & 0 \\
0 & 0 & 0 & 0 & 0 & 0 & 0 & 0 & 0 & 0 & 1 & 0 \\
0 & 0 & 0 & 0 & 0 & 0 & 0 & 0 & 0 & 0 & 0 & 1 \\
0 & 0 & 0 & 0 & -9.78 & 0 & -0.1132 & -0.0110 & -1.2 & 0 & -59.4 & 0 \\
0 & 0 & 0 & 9.78 & 0 & 0 & 0 & -2.2771 & 0 & 59.4 & 0 & -677.9 \\
0 & 0 & 0 & 0 & 0 & 0 & 1.0785 & 0 & -2.1932 & 0 & 677.9 & 0 \\
0 & 0 & 0 & 0 & 0 & 0 & 0 & 0.7031 & 0 & -2.6607 & 0 & 0 \\
0 & 0 & 0 & 0 & 0 & 0 & 0.0739 & 0 & -1.7317 & 0 & -2.7959 & 0 \\
0 & 0 & 0 & 0 & 0 & 0 & 0 & 1.8539 & 0 & -1.1774 & 0 & -2.7959
\end{bmatrix}
\begin{bmatrix} x \\ y \\ z \\ \phi \\ \theta \\ \psi \\ u \\ v \\ w \\ p \\ q \\ r \end{bmatrix}
+
\begin{bmatrix}
\multicolumn{4}{c}{zeros(6x4)} \\
0 & -1.90 & 0 & X_T \\
-0.26 & 0 & -3.23 & 0 \\
0 & 3.18 & 0 & Z_T \\
236.6 & 0 & 10.63 & 0 \\
0 & 15.52 & 0 & M_T \\
2.32 & 0 & 15.87 & 0
\end{bmatrix}
\begin{bmatrix} \delta_p \\ \delta_q \\ \delta_r \\ \delta_T \end{bmatrix}
\tag{A-1}
$$

Table A-3 Sensitivity matrix for linear model example (body-axis)

	λ_1, λ_2 -2.7726 $\pm$ 34.86i		λ_3, λ_4 -2.5102 $\pm$ 34.348i		λ_5 -2.196 + 0i	λ_6 0.00717 + 0i	λ_7 -0.1667 + 0i	λ_8 0.0846 + 0i
ϕ	8.0782e-05	8.0782e-05	2.6222e-21	2.6222e-21	7.0315e-04	**0.9993**	1.5466e-19	3.5879e-19
θ	1.8731e-23	1.8731e-23	1.1057e-05	1.1057e-05	2.1609e-22	5.1315e-19	**0.3395**	**0.6605**
u	5.4889e-20	5.4889e-20	0.0025	0.0025	5.1230e-20	2.6018e-22	**0.6599**	**0.3351**
v	**0.4999**	**0.4999**	1.4197e-18	1.4197e-18	2.2880e-04	1.9910e-05	1.0537e-22	1.5251e-22
w	1.3874e-18	1.3874e-18	**0.4981**	**0.4981**	5.0394e-21	2.4298e-22	5.4253e-05	0.0038
p	0.0184	0.0184	6.8488e-20	6.8488e-20	**1.0307**	0.0034	2.8657e-20	2.5419e-20
q	1.4078e-18	1.4078e-18	**0.4994**	**0.4994**	2.6953e-21	5.3419e-23	6.6820e-04	4.9756e-04
r	**0.5171**	**0.5171**	1.4906e-18	1.4906e-18	0.0316	0.0027	6.1723e-22	1.5908e-20

Bold numbers indicate dominant terms

1 (PDF)	DEFENSE TECHNICAL INFORMATION CTR DTIC OCA
1 (PDF)	DEVCOM ARL FCDD RLB CI TECH LIB
18 (PDF)	DEVCOM ARL FCDD RLA CL F FRESCONI FCDD RLA W T SHEPPARD FCDD RLA WA E BYRD FCDD RLA WB J SADLER FCDD RLA WC M MINNICINO FCDD RLA WD J BRYSON B BURCHETT I CELMINS J DESPIRITO L FAIRFAX B GRUENWALD J PAUL L STROHM J VASILE FCDD RLA WE M ILG J MALEY B TOPPER FCDD RLA WF E RIGAS